

Painting Many Pasts: Synthesizing Time Lapse Videos of Paintings

Amy Zhao
MIT

xamyzhao@mit.com

Frédo Durand
MIT

fredo@mit.edu

Guha Balakrishnan
MIT

balakg@mit.edu

John V. Guttag
MIT

guttag@mit.edu

Kathleen M. Lewis
MIT

kmlewis@mit.edu

Adrian V. Dalca
MIT, MGH

adalca@mit.edu

Abstract

We introduce a new video synthesis task: synthesizing time lapse videos depicting how a given painting might have been created. Artists paint using unique combinations of brushes, strokes, colors, and layers. There are often many possible ways to create a given painting. Our goal is to learn to capture this rich range of possibilities.

Creating distributions of long-term videos is a challenge for learning-based video synthesis methods. We present a probabilistic model that, given a single image of a completed painting, recurrently synthesizes steps of the painting process. We implement this model as a convolutional neural network, and introduce a training scheme to facilitate learning from a limited dataset of painting time lapses. We demonstrate that this model can be used to sample many time steps, enabling long-term stochastic video synthesis. We evaluate our method on digital and watercolor paintings collected from video websites, and show that human raters find our synthesized videos to be similar to time lapses produced by real artists.

1. Introduction

Aspiring artists often learn their craft by following step-by-step tutorials. There are many tutorials that describe how to paint common scenes, but how does one learn to create novel pieces without such guidance? For instance, how might an artist paint a unique fantasy landscape, or mimic the striking style of Paul Cezanne? We present a new video synthesis problem: *given a completed painting, can we synthesize a time lapse video depicting how an artist might have painted it?*

Artistic time lapses present many challenges for video synthesis methods. There is a great deal of variation in how people create art. Suppose two artists are asked to paint the same landscape. One artist might start with the sky, while

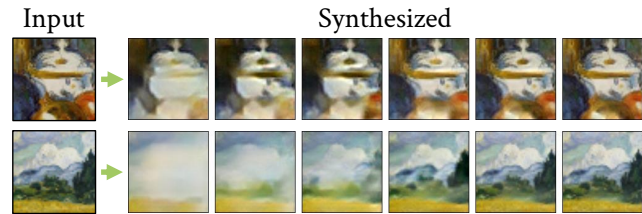


Figure 1: We present a probabilistic model for synthesizing time lapse videos of paintings. We demonstrate our model on *Still Life with a Watermelon and Pomegranates* by Paul Cezanne (top), and *Wheat Field with Cypresses* by Vincent van Gogh (bottom).

the other might start with the mountains in the distance. One might finish each object before moving onto the next, while the other might work a little at a time on each object. During the painting process, there are often few visual cues indicating where the artist will apply the next stroke. The painting process is also long, often spanning hundreds of paint strokes and dozens of minutes.

In this work, we present a solution to the painting time lapse synthesis problem. We begin by defining the problem and describing its unique challenges. We then derive a principled, learning-based model to capture a distribution of steps that a human might use to create a given painting. We introduce a training scheme that encourages the method to produce realistic changes over many time steps. We demonstrate that our model can learn to solve this task, even when trained using a small, noisy dataset of painting time lapses collected from the web. We show that human evaluators almost always prefer our method to an existing video synthesis baseline, and often find our results indistinguishable from time lapses produced by real artists.

This work presents several technical contributions:

1. We demonstrate the use of a probabilistic model to capture stochastic decisions made by artists, thereby captur-

ing a distribution of plausible ways to create a painting.

2. Unlike work in future frame prediction or frame interpolation, we synthesize long-term videos spanning dozens of time steps and many real-time minutes.
3. We demonstrate a model that successfully learns from painting time lapses “from the wild.” This data is small and noisy, having been collected from uncontrolled environments with variable lighting, spatial resolution and video capture rates.

2. Related work

To the best of our knowledge, this is the first work that models and synthesizes distributions of videos of the past, given a single final frame. The most similar work to ours is a recent method called *visual deprojection* [5]. Given a single input image depicting a temporal aggregation of frames, their model captures a distribution of videos that could have produced that image. We compare our method to theirs in our experiments. Here, we review additional related literature in three main areas: video prediction, interpolation, and art synthesis.

2.1. Future frame prediction

Future video frame prediction is the problem of predicting the next frame or few frames of a video, given a sequence of past frames. Early work in this area focused on predicting motion trajectories [8, 16, 34, 50, 54] or synthesizing motions in small frames [40, 41, 49]. Recent methods train convolutional neural networks on large video datasets to synthesize videos of natural scenes and human actions [35, 38, 45, 51, 52]. Zhou *et al.* synthesize time lapse videos, but output only a few frames depicting specific physical processes: melting, rotting, or flowers blooming [68].

Our problem differs from these works in several key ways. First, most future frame prediction methods focus on short time scales, synthesizing frames on the order of seconds into the future, and encompassing relatively small changes. In contrast, painting time lapses span minutes or even hours, and depict dramatic content changes over time. Second, most future frame predictors output a single most likely sequence, making them ill-suited for capturing a variety of very different plausible painting trajectories. One study [62] uses a conditional variational autoencoder to model a distribution of plausible future frames of moving humans. We build upon these ideas to model paint strokes across multiple time steps. Finally, future frame prediction methods focus on natural videos, which depict motions of people and objects [51, 52, 62] or physical processes [68]. The input frames often contain visual cues about how the motion, action or physical process will progress, limiting the space of possibilities that must be captured. In contrast,

snapshots of paintings provide few visual cues, leading to many plausible trajectories.

2.2. Frame interpolation

Our problem can be thought of as a long-term frame interpolation task between a blank canvas and a completed work of art, with many possible painting trajectories between them. In frame interpolation, the goal is to temporally interpolate between two frames in time. Classical approaches focus on natural videos, and estimate dense flow fields [4, 57, 64] or phase [39] to guide the interpolation process. More recent methods use convolutional neural networks to directly synthesize the interpolated frame [44], or combine flow fields with estimates of scene information [28, 43]. Most frame interpolation methods predict a single or a few intermediate frames, and are not easily extended to predicting long sequences, or predicting distributions of sequences.

2.3. Art synthesis

The graphics community has long been interested in simulating physically realistic paint strokes in digital media. Many existing methods focus on physics-based models of fluids or brush bristles [6, 7, 9, 12, 56, 61]. More recent learning-based methods leverage datasets of real paint strokes [31, 36, 67], often posing the artistic stroke synthesis problem as a texture transfer or style transfer problem [3, 37]. Several works focus on simulating watercolor-specific effects such as edge darkening [42, 55]. We focus on capturing large-scale, long-term painting processes, rather than fine-scale details of individual paint strokes.

In style transfer, images are transformed to simulate a specific style, such as a painting-like style [20, 21] or a cartoon-like style [66]. More recently, neural networks have been used for generalized artistic style transfer [18, 69]. We leverage insights from these methods to synthesize a realistic progressions of paintings.

Several recent works use reinforcement learning by first designing parameterized brush strokes, and then training an agent to apply strokes to produce a given painting [17, 22, 26, 27, 58, 59]. Some works focus on specific artistic tasks such as hatching or other repetitive strokes [29, 60]. These approaches require careful hand-engineering, and are not ++optimized to produce varied or realistic painting progressions. In contrast, we learn a broad set of effects from real painting time lapse data.

3. Problem overview

Given a completed painting, our goal is to synthesize different ways that an artist might have created it. We work with recordings of digital and watercolor painting time lapses collected from video websites. Compared to

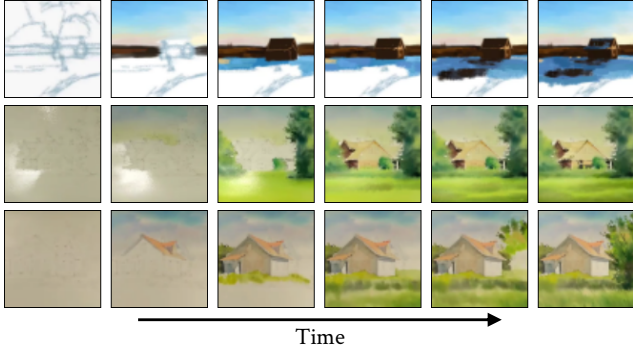


Figure 2: Several real painting progressions of similar-looking scenes. Each artist fills in the house, sky and field in a different order.

natural videos of scenes and human actions, videos of paintings present unique challenges.

High Variability

Painting trajectories: Even for the same scene, different artists will likely paint objects in different temporal orders (Figure 2).

Painting rates: Artists work at different speeds, and apply paint in different amounts.

Scales and shapes: Over the course of a painting, artists use strokes that vary in size and shape. Artists often use broad strokes early on, and add fine details later.

Data availability: Due to the limited number of available videos in the wild, it is challenging to gather a dataset that captures the aforementioned types of variability.

Medium-specific challenges

Non-paint effects: Tools that apply local blurring, smudging, or specialized paint brush shapes are common in digital art applications such as Procreate [23]. Artists can also apply global effects simulating varied lighting or tones.

Erasing effects: In digital art programs, artists can erase or undo past actions, as shown in Figure 3.

Physical effects in watercolor paintings: Watercolor painting videos exhibit distinctive effects resulting from the physical interaction of paint, water, and paper. These effects include specular lighting on wet paint, pigments fading as they dry, and water spreading from the point of contact with the brush (Figure 4).

In this work, we design a learning-based model to handle the challenges of high variability and painting medium-specific effects.

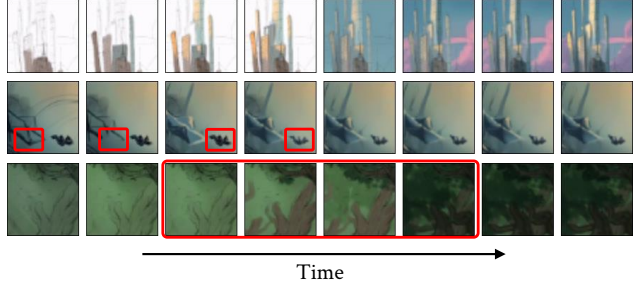


Figure 3: Example digital painting sequences. These sequences show a variety of ways to add paint, including fine strokes and filling (row 1), and broad strokes (row 3). We use red boxes to outline challenges, including erasing (row 2) and drastic changes in color and composition (row 3).

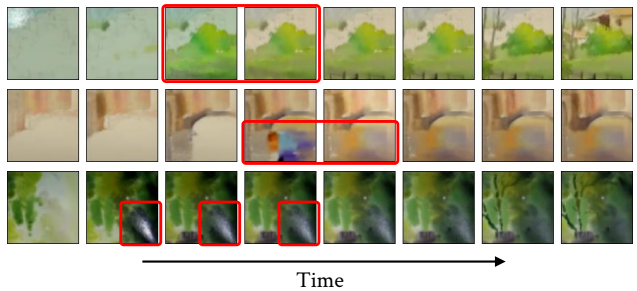


Figure 4: Example watercolor painting sequences. The outlined areas highlight some watercolor-specific challenges, including changes in lighting (row 1), diffusion and fading effects as paint dries (row 2), and specular effects on wet paint (row 3).

4. Method

We begin by formalizing the time lapse video synthesis problem. Given a painting x_T , our task is to synthesize the past frames x_1, \dots, x_{T-1} . Suppose we have a training set of real time lapse videos $\{\mathbf{x}^{(i)} = x_1^{(i)}, \dots, x_{T^{(i)}}^{(i)}\}$. We first define a principled probabilistic model, and then learn its parameters using these videos. At test time, given a completed painting, we sample from the model to create new videos that show realistic-looking painting processes.

4.1. Model

We propose a probabilistic, temporally recurrent *paint strokes model*. At each time instance t , the model predicts a pixel-wise intensity change δ_t that should be added to the previous frame to produce the current frame; that is, $x_t = x_{t-1} + \delta_t$. This change does not necessarily correspond to a single paint stroke – it could represent one or multiple physical or digital paint strokes, or other effects such as erasing or fading.

We model δ_t as being generated from a random latent variable z_t , the completed piece x_T , and the image

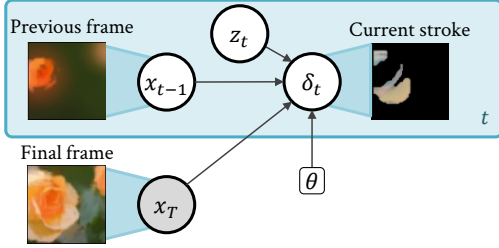


Figure 5: We model the change δ_t at each time step as being generated from the latent variable z_t . Circles represent random variables; the shaded circle denotes a variable that is observed at inference time. The rounded rectangle represents model parameters.

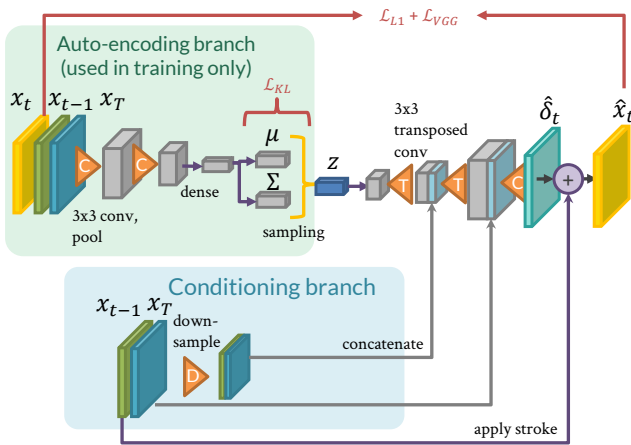


Figure 6: We implement our model using a conditional variational autoencoder framework. At training time, the network is encouraged to reconstruct the current frame x_t , while sampling the latent z_t from a distribution that is close to the standard normal. At test time, the auto-encoding branch is removed, and z_t is sampled from the standard normal. We use the shorthand $\hat{\delta}_t = g_\theta(z_t, x_{t-1}, x_T)$, $\hat{x}_t = x_{t-1} + \hat{\delta}_t$.

content at the previous time step x_{t-1} ; the likelihood is $p_\theta(\delta_t | z_t, x_{t-1}; x_T)$. Using a random variable z_t helps to capture the stochastic nature of painting. Using both x_T and x_{t-1} enables the model to capture time-varying effects such as the progression of coarse to fine brush sizes, while the Markovian assumption facilitates learning from a small number of video examples.

It is common to define such image likelihoods as a per-pixel normal distribution, which results in an L2 image similarity loss term in maximum likelihood formulations [33]. In synthesis tasks, using L2 loss often produces blurry results [24]. We instead optimize both the L1 distance in pixel space and the L2 distance in a perceptual feature space. Per-

ceptual losses are commonly used in image synthesis and style transfer tasks to produce sharper and more visually pleasing results [14, 24, 30, 44, 65]. We use the L2 distance between normalized VGG features [48] as described in [65]. We let the likelihood take the form:

$$p_\theta(\delta_t | z_t, x_{t-1}; x_T) \propto e^{-\frac{1}{\sigma_1^2} |\delta_t - \hat{\delta}_t|} \mathcal{N}(V(x_{t-1} + \delta_t); V(x_{t-1} + \hat{\delta}_t), \sigma_2^2 \mathbb{I}), \quad (1)$$

where $\hat{\delta}_t = g_\theta(z_t, x_{t-1}, x_T)$, $g_\theta(\cdot)$ represents a function parameterized by θ , $V(\cdot)$ is a function that extracts normalized VGG features, and σ_1, σ_2 are fixed noise parameters.

We assume the latent variable z_t is generated from the multivariate standard normal distribution:

$$p(z_t) = \mathcal{N}(z_t; 0, \mathbb{I}). \quad (2)$$

We show a diagram of this model in Figure 5.

We aim to find model parameters θ that best explain all videos in our dataset:

$$\begin{aligned} & \arg \max_{\theta} \prod_i \prod_t p_\theta(\delta_t^{(i)}, x_{t-1}^{(i)}, x_T^{(i)}) \\ & = \arg \max_{\theta} \prod_i \prod_t \int_{z_t} p_\theta(\delta_t^{(i)} | z_t^{(i)}, x_{t-1}^{(i)}; x_T^{(i)}) dz_t. \end{aligned} \quad (3)$$

This integral is intractable, and the posterior $p(z_t | \delta_t, x_{t-1}; x_T)$ is also intractable, preventing the use of the EM algorithm. We instead use variational inference and introduce an approximate posterior distribution $p(z_t | \delta_t, x_{t-1}; x_T) \approx q_\phi(z_t | \delta_t, x_{t-1}; x_T)$ [32, 62, 63]. We let this approximate distribution take the form of a multivariate normal:

$$\begin{aligned} & q_\phi(z_t | \delta_t, x_{t-1}, x_T) \\ & = \mathcal{N}(z_t; \mu_\phi(\delta_t, x_{t-1}, x_T), \Sigma_\phi(\delta_t, x_{t-1}, x_T)), \end{aligned} \quad (4)$$

where $\mu_\phi(\cdot), \Sigma_\phi(\cdot)$ are functions parameterized by ϕ , and $\Sigma_\phi(\cdot)$ is diagonal.

4.1.1 Neural network framework

We implement the functions g_θ , μ_ϕ and Σ_ϕ as a convolutional encoder-decoders parameterized by θ and ϕ , using a conditional variational autoencoder (CVAE) framework [53, 63]. We use an architecture similar to [63], which we summarize in Figure 6. We include full details in the appendix.

4.2. Learning

We learn model parameters using short sequences from the training video dataset, which we discuss in further detail in Section 5.1. We use two stages of optimization to facilitate convergence: pairwise optimization, and sequence optimization.

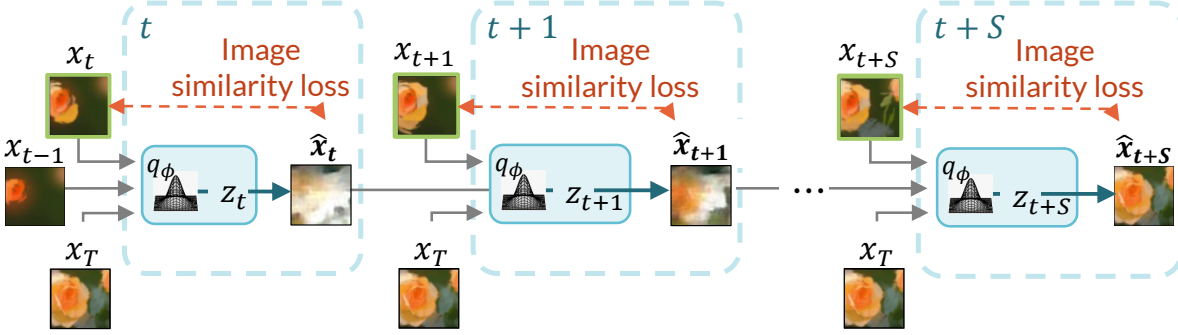


Figure 7: In sequential CVAE training, our model is trained to reconstruct a training frame (outlined in green) while building upon its previous predictions for S time steps.

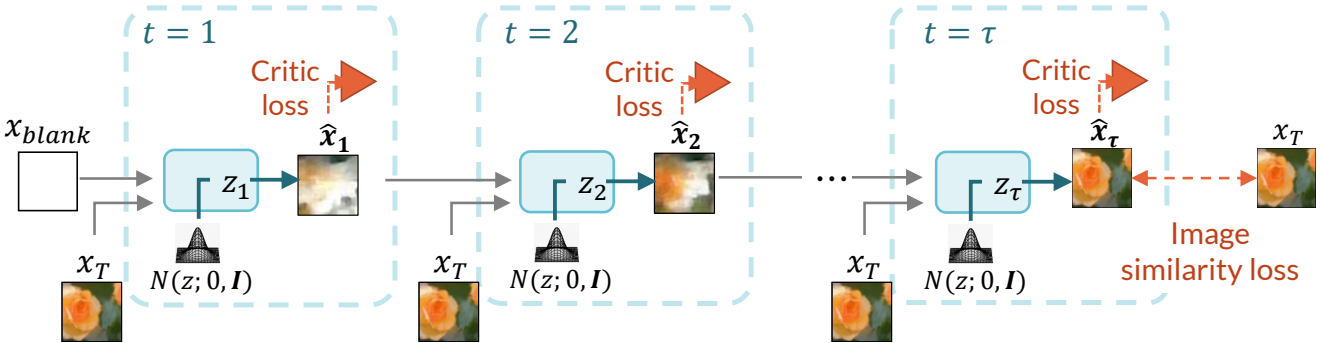


Figure 8: In sequential sampling training, we use a conditional frame critic to encourage all frames sampled from our model to look realistic. The image similarity loss on the final frame encourages the model to complete the painting in τ time steps.

4.2.1 Pairwise optimization

From Equations (3) and (4), we obtain an expression for each *pair* of consecutive frames (a derivation is provided in the appendix):

$$\begin{aligned} & \log p_\theta(\delta_t, x_{t-1}, x_T) \\ & \geq \mathbb{E}_{z_t \sim q_\phi(z_t | x_{t-1}, \delta_t; x_T)} [\log p_\theta(\delta_t | z_t, x_{t-1}; x_T)] \\ & \quad - KL[q_\phi(z_t | \delta_t, x_{t-1}; x_T) || p(z_t)], \end{aligned} \quad (5)$$

where $KL[\cdot || \cdot]$ denotes the Kullback-Liebler divergence. Combining Equations (1), (2), (4), and (5), we minimize:

$$\begin{aligned} & \mathcal{L}_{KL} + \frac{1}{\sigma_1^2} \mathcal{L}_{L1}(\delta_t, \hat{\delta}_t) \\ & + \frac{1}{2\sigma_2^2} \mathcal{L}_{L2}(VGG(x_{t-1} + \delta_t), VGG(x_{t-1} + \hat{\delta}_t)), \end{aligned} \quad (6)$$

where $\mathcal{L}_{KL} = \frac{1}{2}(-\log \Sigma_\phi + \Sigma_\phi + \mu_\phi^2)$, and $\mathcal{L}_{L1}, \mathcal{L}_{L2}$ represent L1 and L2 distance respectively. We refer to the last two terms as image similarity losses.

We optimize Equation (6) on single time steps, which we obtain by sampling all pairs of consecutive frames from the dataset. We also train the model to produce the first frame x_1 from videos that begin with a blank canvas, given a white

input frame x_{blank} , and x_T . These *starter sequences* are important for teaching the model how to start a painting at inference time.

4.2.2 Sequence optimization

To synthesize an entire video, we run our model recurrently for multiple time steps, building upon its own predicted frames. It is common when making sequential predictions to observe compounding errors or artifacts over time [51]. We use a novel sequential training scheme to enforce that the outputs of the model are accurate and realistic over multiple time steps. We alternate between two sequential training modes.

Sequential CVAE training encourages *sequences* of frames to be well-captured by the learned distribution, by reducing the compounding of errors. Specifically, we train the model sequentially for a few frames, predicting each intermediate frame \hat{x}_t using the output of the model at the previous time step: $\hat{x}_t = \hat{x}_{t-1} + \hat{\delta}_t$. We compare each predicted frame to the corresponding training frame using the image similarity losses in Eq. (6). We illustrate this strategy in Figure 7.

Sequential sampling training encourages random samples from our learned distribution to look like realistic partially-completed paintings. During inference (described below), we rely on sampling from the prior $p(z_t)$ at each time step to synthesize new videos. A limitation of the variational strategy is the limited coverage of the latent space z_t during training [15], sometimes leading to unrealistic predictions $\hat{x}_t = \hat{x}_{t-1} + g_\theta(z_t, \hat{x}_{t-1}, x_T)$ for $z_t \sim p(z_t)$. To compensate for this, we introduce supervision on such samples by amending the reconstruction term in Equation (5) using a conditional critic loss term [19]:

$$\begin{aligned} \mathcal{L}_{critic} &= \mathbb{E}_{z_t \sim p(z_t)} [D_\psi(\hat{x}_t, \hat{x}_{t-1}, x_T)] \\ &\quad - \mathbb{E}_{x_t} [D_\psi(x_t, x_{t-1}, x_T)], \end{aligned} \quad (7)$$

where $D_\psi(\cdot)$ is a critic function with parameters ψ . The critic encourages the distribution of sampled strokes $\hat{\delta}_t = g_\theta(z_t, \hat{x}_{t-1}, x_T)$, $z_t \sim p(z_t)$ to match the distribution of training strokes δ_t . We use a critic architecture based on [10] and optimize it using WGAN-GP [19].

In addition to the critic loss, we apply the image similarity losses discussed above after τ time steps, to encourage the model to eventually produce the completed painting.

4.3. Inference: video synthesis

Given a completed painting x_T and learned model parameters θ, ϕ , we synthesize videos by sampling from the model at each time step. Specifically, we synthesize each frame $\hat{x}_t = \hat{x}_{t-1} + g_\theta(z_t, \hat{x}_{t-1}, x_T)$ using the synthesized previous frame \hat{x}_{t-1} and a randomly sampled $z_t \sim p(z_t)$. We start each video using $\hat{x}_0 = x_{blank}$, a blank frame.

4.4. Implementation

We implement our model using Keras [11] and Tensorflow [1]. We experimentally selected the hyperparameters controlling the reconstruction loss weights to be $\sigma_1 = \sigma_2 = 0.1$, using the validation set.

5. Experiments

5.1. Datasets

We collected recordings of painting time lapses from YouTube and Vimeo. We selected digital and watercolor paintings (which are common painting methods on these websites), and focused on landscapes or still lifes (which are common subjects for both mediums). We downloaded each video at 360×640 resolution and cropped it temporally and spatially to include only the painting process (excluding any introductions or sketching that might have preceded the painting). We split each dataset in a 70:15:15 ratio into

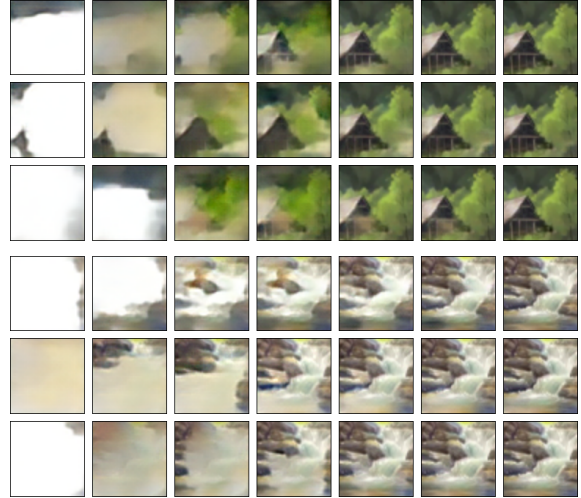


Figure 9: **Diversity of sampled videos.** We show examples of our method applied to a digital (top 3 rows) and a watercolor (bottom 3 rows) painting from the test set. Our method captures diverse and plausible painting trajectories.

training, validation, and held-out test video sets.¹

Digital paintings: We collected 117 digital painting time lapses. The average duration is 4 minutes, with many videos having already been sped up by artists using the Procreate application [23]. We selected videos with minimal zooming and panning. We manually removed segments that contained movements such as translations, flipping and zooming. Figure 3 shows example video sequences.

Watercolor paintings: We collected 116 watercolor time lapses, with an average duration of 20 minutes. We only kept videos that contained minimal movement of the paper, and manually corrected any small translations of the painting. We show examples in Figure 4.

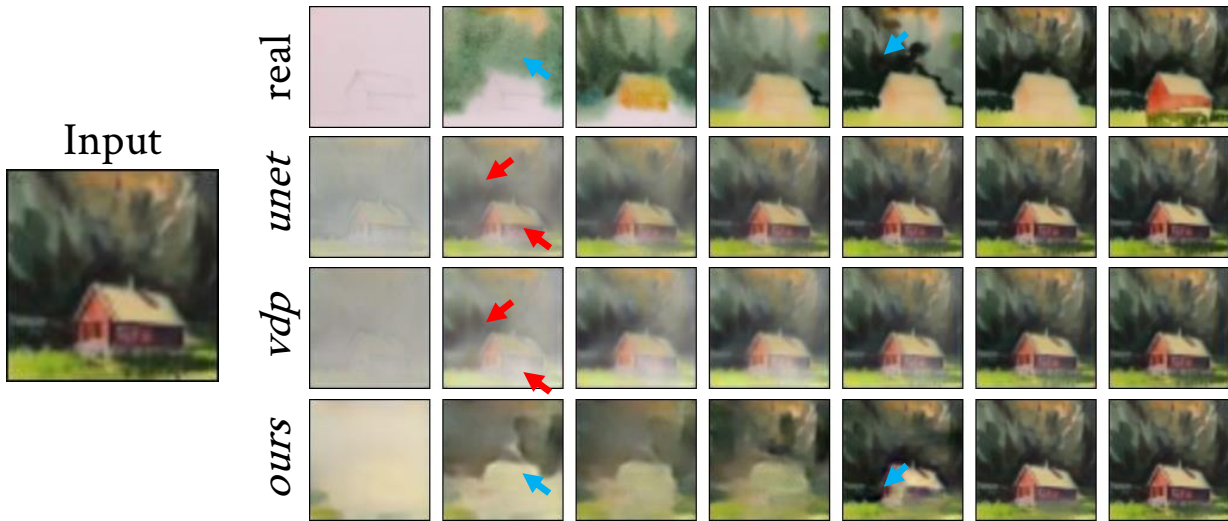
A challenge with videos of physical paintings is the presence of the hand, paintbrush and shadows in many frames. We trained a simple convolutional neural network to identify and remove frames that contained these artifacts.

Sequence extraction. We synthesize time lapses at a lower temporal resolution than real-time for computational feasibility. We extract training sequences from the raw videos at a period of $\gamma > 0$ frames (*i.e.*, skipping γ real frames in each synthesized time step), with a maximum variance of ϵ frames. Allowing some variance in the sampling rate enables us to extract sequences at an *approximate* period of γ frames, which is useful for (1) improving robustness to varied painting rates, and (2) extracting sequences from watercolor painting videos where many frames containing

¹While we cannot host individual video files, we make our download scripts available at <https://xamy Zhao.github.io/timecraft>.



(a) **Similarly to the artist, our method paints in a coarse-to-fine manner.** Blue arrows show where our method first applies a flat color, and then adds fine details. Red arrows indicate where the baselines add fine details even in the first time step.



(b) **Our method works on similar regions to the artist, although it does not use the same color layers to achieve the completed painting.** Blue arrows show where our method paints similar parts of the scene to the artist (filling in the background first, and then the house, and then adding details to the background). Red arrows indicate where the baselines do not paint according to semantic boundaries, filling in both the background and the house.

Figure 10: Videos predicted from the digital (top) and watercolor (bottom) test sets. For the stochastic methods *vdp* and *ours*, we show the nearest sample to the real video out of 2000 samples. We show additional results in the appendices.

hands or paintbrushes have been removed. We select γ and ϵ independently for each dataset. We avoid capturing static segments of each video (e.g., when the artist is speaking) by requiring that adjacent frames in each sequence have at least 1% of the pixels changing by a fixed intensity threshold. We use a dynamic programming method to find all sequences that satisfy these criteria. We train on sequences of length 3 or 5 for sequential CVAE training, and length $\tau = 40$ for sequential sampling training, which we deter-

mined using experiments on the validation set. For the test set, we extract a single sequence from each test video that satisfies the filtering criteria.

Crop extraction. To facilitate learning from small numbers of videos, we extract multiple 50×50 crops from each video. We first downsample each video spatially by a factor of 0.6, so that most patches contained visually interesting content and spatial context.

Comparison	All paintings	Watercolor paintings	Digital paintings
real > <i>vdp</i>	90%	90%	90%
real > <i>ours</i>	55%	60%	51%
<i>ours</i> > <i>vdp</i>	91%	90%	88%

Table 1: **User study results.** Users compared the realism of pairs of videos randomly sampled from *ours*, *vdp*, and real videos. The vast majority of participants preferred our videos over *vdp* videos ($p < 0.0001$). Similarly, most participants chose real videos over *vdp* videos ($p < 0.0001$). Users preferred real videos over *ours* ($p = 0.0004$), but many participants confused our videos with the real videos, especially for digital paintings.

5.2. Baselines

We compare our method to the following baselines:

Deterministic video synthesis (*UNET*): In image synthesis tasks, it is common to use a simple encoder-decoder architecture with skip connections, similar to U-Net [24, 46]. We adapt this technique to synthesize the entire video at once.

Stochastic video synthesis (*vdp*): Visual deprojection synthesizes a distribution of videos from a single temporally-projected input image [5].

We design each baseline model architecture to have a comparable number of parameters to our model. Both baselines output videos of a fixed length, which we choose to be 40 to be comparable to our choice of $\tau = 40$ in Section 5.1.

5.3. Results

We conducted both quantitative and qualitative evaluations. We first present a user study quantifying human perception of the realism of our synthesized videos. Next, we qualitatively examine our synthetic videos, and discuss characteristics that contribute to their realism. Finally, we discuss quantitative metrics for comparing sets of sampled videos to real videos. We show additional results, including videos and visualizations using the tipix tool [13] on our project page at <https://xamyzhao.github.io/timecraft>.

We experimented with training each method on digital or watercolor paintings only, as well as on the combined paintings dataset. For all methods, we found that training on the combined dataset produced the best qualitative and quantitative results (likely due to our limited dataset size), and we only present results for those models.

5.3.1 Human evaluations

We surveyed 158 people using Amazon Mechanical Turk [2]. Participants compared the realism of pairs of videos, with each pair containing videos randomly sampled

from *ours*, *vdp*, or the real videos. In this study, we omit the weaker baseline *UNET*, which performed consistently worse on all metrics (discussed below).

We first trained the participants by showing them several examples of real painting time lapses. We then showed them a pair of time lapse videos generated by different methods for the center crop of the same painting, and asked “Which video in each pair shows a more realistic painting process?” We repeated this process for 14 randomly sampled paintings from the combined test set. We include full study details in the appendix. Table 1 indicates that almost every participant thought synthetic videos produced by our model looked more realistic than those produced by *vdp* ($p < 0.0001$). Furthermore, participants confused our synthetic videos with real videos nearly half of the time. In the next sections, we show example synthetic videos and discuss aspects that make the results of our model appear more realistic, offering an explanation for these promising user study results.

5.3.2 Qualitative results

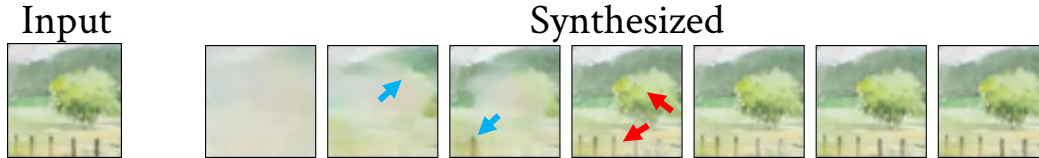
Figure 9 shows sample sequences produced by our model, for two input paintings. Our model chooses different orderings of semantic regions from the beginning of each sequence, leading to different paths that still converge to the same completed painting.

Figure 10 shows sequences synthesized by each method. To objectively compare the stochastic methods *vdp* and *ours*, we show the most similar prediction by L1 distance to the ground truth sequence. The ground truth sequences show that artists tend to paint in a coarse-to-fine manner, using broad strokes near the start of a painting, and finer strokes near the end. As we highlight with arrows, our method captures this tendency better than baselines, having learned to focus on separate semantic regions such as mountains, cabins and trees. Our predicted trajectories are similar to the ground truth, showing that our sequential modeling approach is effective at capturing realistic temporal progressions. In contrast, the baselines tend to make blurry changes without separating the scene into components, a common result for methods that do not explicitly model stochastic processes.

We examine failure cases from our method in Figure 11, such as making many fine or disjoint changes in a single time step and creating an unrealistic effect.

5.3.3 Quantitative results

Comparing synthesized results to “ground truth” in a stochastic task is ill-defined, and developing quantitative measures of realism is difficult [25, 47]; these challenges motivated our user study above. In this section, we explore quantitative metrics designed to measure aspects of time



(a) **The proposed method does not always synthesize realistic strokes for fine details.** Blue arrows highlight frames where the method makes realistic paint strokes, working in one or two semantic regions at a time. Red arrows show how our method sometimes fills in many details in the frame at once.



(b) **The proposed method sometimes synthesizes changes in disjoint regions.** Red arrows indicate where the method produces paint stroke samples that fill in small patches that correspond to disparate semantic regions, leaving unrealistic blank gaps throughout the frame. Like the previous example, this example also fills in much of the frame in one time step, although most of the filled areas in the second frame are coarse.

Figure 11: **Failure cases.** We show unrealistic effects that are sometimes synthesized by our method, for a watercolor painting (top) and a digital painting (bottom).

lapse realism. For each video in the test set, we extract a 40-frame long sequence according to the criteria described in Section 5.1, and evaluate each method on 5 random crops using several video similarity metrics:

Best (across k samples) overall video similarity: For each test painting, we draw k sample videos from each model and report the closest sample to the true video using a per-pixel L1 loss [5]. A method that has captured the distribution of real time lapses well should produce better “best” estimates as $k \rightarrow \infty$. This captures whether some samples drawn from a model get close to the real video, and also whether a method is diverse enough to capture each artist’s specific choices.

Best (across k samples) stroke shape similarity: We quantify how similar the set of stroke shapes are between the ground truth and each predicted video, disregarding the order in which they were performed. We define *stroke shape* as a binary map of the changes made in each time step. For each test video, we compare the artist’s stroke shape to the most similarly shaped stroke synthesized by each method, as measured by intersection-over-union (IOU), and report the average IOU over all ground truth strokes. This captures whether a method paints in similar semantic regions to the artist.

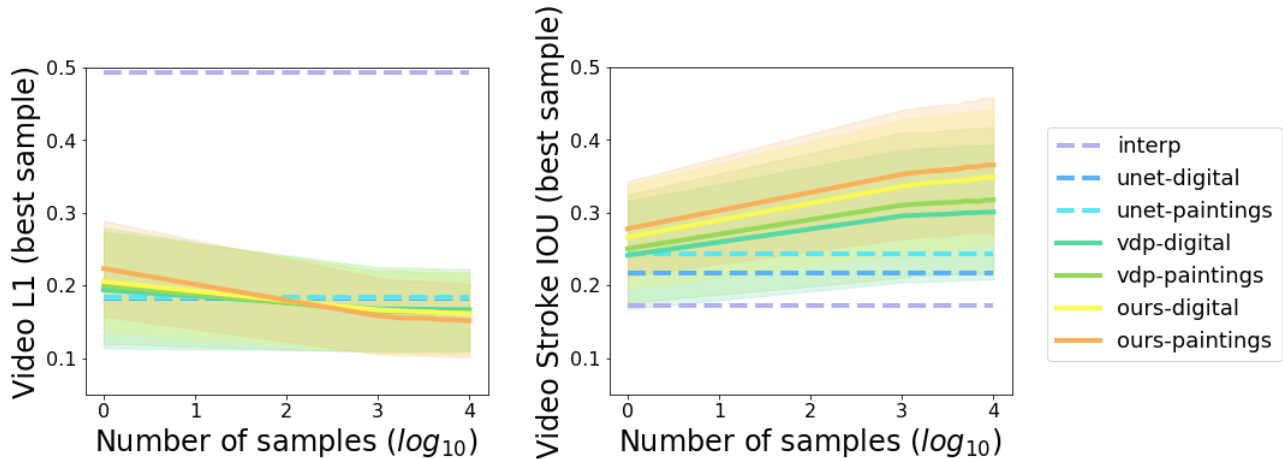
In Table 2 we introduce the *interp* baseline, which linearly interpolates in time, as a quantitative lower bound. For $k = 2000$, the deterministic *interp* and *unet* approaches perform poorly for both metrics. *vdp* and our method are

able to produce samples that lead to comparable “best video similarity”, highlighting the strength of methods designed to capture distributions of videos. The stroke IOU metric shows that our method synthesizes strokes that are significantly more realistic than the other methods.

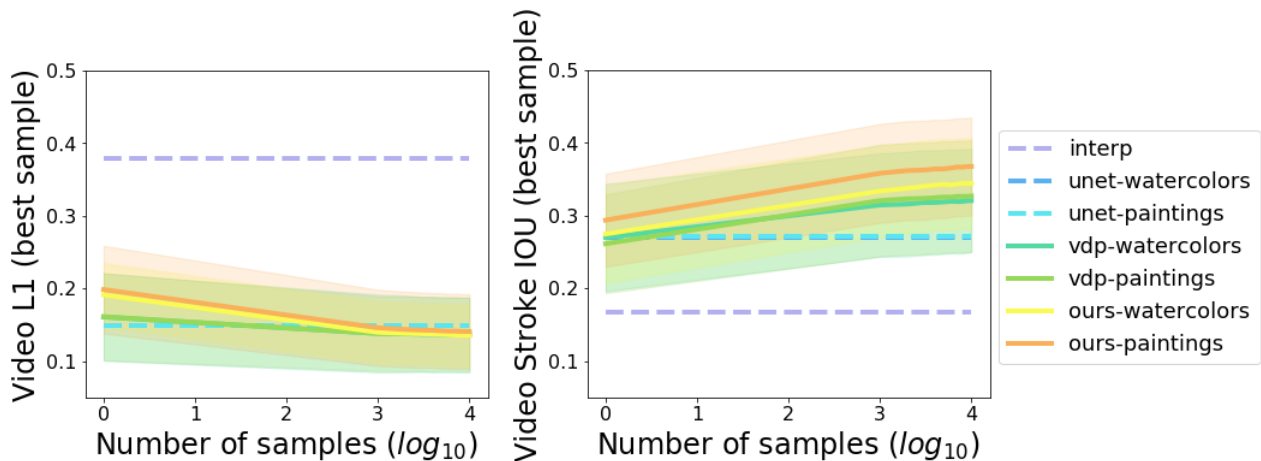
We show the effect of increasing k in Figure 12. At low k , the blurry videos produced by *interp* and *unet* attain lower L1 distance to the real video than *vdp* and *ours*, likely because L1 distance penalizes samples with different painting progressions more than it penalizes blurry frames. In other words, a blurry, gradually fading video with “average” frames will typically have a lower L1 distance to the artist’s time lapse, compared to different plausible painting processes. As k increases, *vdp* and *ours* produce some samples that are close to the real video. Together with the user study described above, these metrics illustrate encouraging results that our method captures a realistic variety of painting time lapses.

6. Conclusion

In this work, we introduce a new video synthesis problem: making time lapse videos that depict the creation of paintings. We proposed a recurrent probabilistic model that captures the stochastic decisions of human artists. We introduced an alternating sequential training scheme that encourages the model to make realistic predictions over many time steps. We demonstrated our model on digital and watercolor paintings, and used it to synthesize realistic and varied painting videos. Our results, including human evaluations, indicate that the proposed model is a powerful first tool for



(a) Digital paintings test set.



(b) Watercolor paintings test set.

Figure 12: **Quantitative measures.** As we draw more samples from each stochastic method (solid lines), the best video similarity to the real video improves. This indicates that some samples are close to the artist’s specific painting choices. We use L1 distance as the metric on the left (lower is better), and stroke IOU on the right (higher is better). Shaded regions show standard deviations of the stochastic methods. We highlight several insights from these plots. (1) Both our method and *vdp* produce samples that are comparably similar to the real video by L1 distance (left). However, our method synthesizes strokes that are more similar in shape to those used by artists (right). (2) At low numbers of samples, the deterministic *UNET* method is closer (by L1 distance) to the real video than samples from *vdp* or *ours*, since L1 favors blurry frames that average many possibilities. (3) Our method shows more improvement in L1 distance and stroke area IOU than *vdp* as we draw more samples, indicating that our method captures a more varied distribution of videos.

capturing stochastic changes from small video datasets.

7. Acknowledgments

We thank Zoya Bylinskii of Adobe Inc. for her insights around designing effective and accurate user studies. This work was funded by Wistron Corporation.

References

- [1] Martín Abadi et al. Tensorflow: Large-scale machine learning on heterogeneous distributed systems. *arXiv preprint arXiv:1603.04467*, 2016.
- [2] Inc. Amazon Mechanical Turk. Amazon mechanical turk: Overview, 2005.
- [3] Ryoichi Ando and Reiji Tsuruno. Segmental brush synthesis with stroke images. 2010.
- [4] Simon Baker, Daniel Scharstein, JP Lewis, Stefan Roth,

Method	Digital paintings		Watercolor paintings	
	L1	Stroke IOU	L1	Stroke IOU
interp	0.49 (0.13)	0.17 (0.06)	0.38 (0.09)	0.17 (0.09)
unet	0.18 (0.08)	0.24 (0.08)	0.15 (0.06)	0.27 (0.07)
vdp	0.16 (0.06)	0.31 (0.10)	0.14 (0.05)	0.32 (0.08)
ours	0.16 (0.05)	0.36 (0.09)	0.14 (0.05)	0.36 (0.07)

Table 2: We compare videos synthesized from the digital and watercolor painting test sets to the artists’ videos. We include a simple baseline *interp* that linearly interpolates in time between a white frame and the completed painting. For stochastic methods *vdp* and *ours*, we draw 2000 video samples and report the closest one to the ground truth.

Michael J Black, and Richard Szeliski. A database and evaluation methodology for optical flow. *International Journal of Computer Vision*, 92(1):1–31, 2011.

- [5] Guha Balakrishnan, Adrian V. Dalca, Amy Zhao, John V. Guttag, Fredo Durand, and William T Freeman. Visual deprojection: Probabilistic recovery of collapsed dimensions. In *IEEE International Conference on Computer Vision (ICCV)*, 2019.
- [6] William Baxter, Yuanxin Liu, and Ming C Lin. A viscous paint model for interactive applications. *Computer Animation and Virtual Worlds*, 15(3-4):433–441, 2004.
- [7] William V Baxter and Ming C Lin. A versatile interactive 3d brush model. In *Computer Graphics and Applications, 2004. PG 2004. Proceedings. 12th Pacific Conference on*, pages 319–328. IEEE, 2004.
- [8] Maren Bennewitz, Wolfram Burgard, and Sebastian Thrun. Learning motion patterns of persons for mobile service robots. In *Proceedings 2002 IEEE International Conference on Robotics and Automation (Cat. No. 02CH37292)*, volume 4, pages 3601–3606. IEEE, 2002.
- [9] Zhili Chen, Byungmoon Kim, Daichi Ito, and Huamin Wang. Wetbrush: Gpu-based 3d painting simulation at the bristle level. *ACM Transactions on Graphics (TOG)*, 34(6):200, 2015.
- [10] Yunjey Choi, Minje Choi, Munyoung Kim, Jung-Woo Ha, Sunghun Kim, and Jaegul Choo. Stargan: Unified generative adversarial networks for multi-domain image-to-image translation. In *Proceedings of the IEEE Conference on Computer Vision and Pattern Recognition*, pages 8789–8797, 2018.
- [11] François Chollet et al. Keras. <https://github.com/fchollet/keras>, 2015.
- [12] Nelson S-H Chu and Chiew-Lan Tai. Moxi: real-time ink dispersion in absorbent paper. In *ACM Transactions on Graphics (TOG)*, volume 24, pages 504–511. ACM, 2005.
- [13] Adrian V Dalca, Ramesh Sridharan, Natalia Rost, and Polina Golland. tipix: Rapid visualization of large image collections. *MICCAI-IMIC Interactive Medical Image Computing Workshop*.
- [14] Alexey Dosovitskiy and Thomas Brox. Generating images with perceptual similarity metrics based on deep networks. In *Advances in neural information processing systems*, pages 658–666, 2016.
- [15] Jesse Engel, Matthew Hoffman, and Adam Roberts. Latent constraints: Learning to generate conditionally from unconditional generative models. In *International Conference on Learning Representations*, 2018.
- [16] Scott Gaffney and Padhraic Smyth. Trajectory clustering with mixtures of regression models. In *KDD*, volume 99, pages 63–72, 1999.
- [17] Yaroslav Ganin, Tejas Kulkarni, Igor Babuschkin, SM Eslami, and Oriol Vinyals. Synthesizing programs for images using reinforced adversarial learning. *arXiv preprint arXiv:1804.01118*, 2018.
- [18] Leon A Gatys, Alexander S Ecker, and Matthias Bethge. A neural algorithm of artistic style. *arXiv preprint arXiv:1508.06576*, 2015.
- [19] Ishaan Gulrajani, Faruk Ahmed, Martin Arjovsky, Vincent Dumoulin, and Aaron C Courville. Improved training of wasserstein gans. In *Advances in neural information processing systems*, pages 5767–5777, 2017.
- [20] Aaron Hertzmann. Painterly rendering with curved brush strokes of multiple sizes. In *Proceedings of the 25th annual conference on Computer graphics and interactive techniques*, pages 453–460. ACM, 1998.
- [21] Fay Huang, Bo-Hui Wu, and Bo-Ru Huang. Synthesis of oil-style paintings. In *Pacific-Rim Symposium on Image and Video Technology*, pages 15–26. Springer, 2015.
- [22] Zhewei Huang, Wen Heng, and Shuchang Zhou. Learning to paint with model-based deep reinforcement learning. In *IEEE International Conference on Computer Vision (ICCV)*, 2019.
- [23] Savage Interactive. *Procreate Artists’ Handbook*. Savage, 2016.
- [24] Phillip Isola, Jun-Yan Zhu, Tinghui Zhou, and Alexei A Efros. Image-to-image translation with conditional adversarial networks. *arXiv preprint arXiv:1611.07004*, 2016.
- [25] Phillip Isola, Jun-Yan Zhu, Tinghui Zhou, and Alexei A Efros. Image-to-image translation with conditional adversarial networks. In *Proceedings of the IEEE conference on computer vision and pattern recognition*, pages 1125–1134, 2017.
- [26] Biao Jia, Jonathan Brandt, Radomír Mech, Byungmoon Kim, and Dinesh Manocha. Lpaintb: Learning to paint from self-supervision. *CoRR*, abs/1906.06841, 2019.
- [27] Biao Jia, Chen Fang, Jonathan Brandt, Byungmoon Kim, and Dinesh Manocha. Paintbot: A reinforcement learning approach for natural media painting. *CoRR*, abs/1904.02201, 2019.
- [28] Huaizu Jiang, Deqing Sun, Varun Jampani, Ming-Hsuan Yang, Erik Learned-Miller, and Jan Kautz. Super slo-mo: High quality estimation of multiple intermediate frames for video interpolation. In *Proceedings of the IEEE Conference on Computer Vision and Pattern Recognition*, pages 9000–9008, 2018.
- [29] Pierre-Marc Jodoin, Emric Epstein, Martin Granger-Piché, and Victor Ostromoukhov. Hatching by example: a statistical approach. In *Proceedings of the 2nd international symposium on Non-photorealistic animation and rendering*, pages 29–36. ACM, 2002.

- [30] Justin Johnson, Alexandre Alahi, and Li Fei-Fei. Perceptual losses for real-time style transfer and super-resolution. In *European conference on computer vision*, pages 694–711. Springer, 2016.
- [31] Mikyung Kim and Hyun Joon Shin. An example-based approach to synthesize artistic strokes using graphs. In *Computer Graphics Forum*, volume 29, pages 2145–2152. Wiley Online Library, 2010.
- [32] Diederik P Kingma, Shakir Mohamed, Danilo Jimenez Rezende, and Max Welling. Semi-supervised learning with deep generative models. In *Advances in Neural Information Processing Systems*, pages 3581–3589, 2014.
- [33] Diederik P Kingma and Max Welling. Auto-encoding variational bayes. *arXiv preprint arXiv:1312.6114*, 2013.
- [34] Ce Liu, Jenny Yuen, and Antonio Torralba. Sift flow: Dense correspondence across scenes and its applications. *IEEE transactions on pattern analysis and machine intelligence*, 33(5):978–994, 2010.
- [35] Ziwei Liu, Raymond A Yeh, Xiaoou Tang, Yiming Liu, and Aseem Agarwala. Video frame synthesis using deep voxel flow. In *Proceedings of the IEEE International Conference on Computer Vision*, pages 4463–4471, 2017.
- [36] Jingwan Lu, Connelly Barnes, Stephen DiVerdi, and Adam Finkelstein. Realbrush: painting with examples of physical media. *ACM Transactions on Graphics (TOG)*, 32(4):117, 2013.
- [37] Michal Lukáč, Jakub Fišer, Paul Asente, Jingwan Lu, Eli Shechtman, and Daniel Šykora. Brushables: Example-based edge-aware directional texture painting. In *Computer Graphics Forum*, volume 34, pages 257–267. Wiley Online Library, 2015.
- [38] Michael Mathieu, Camille Couprie, and Yann Lecun. Deep multi-scale video prediction beyond mean square error. 11 2016.
- [39] Simone Meyer, Oliver Wang, Henning Zimmer, Max Grosse, and Alexander Sorkine-Hornung. Phase-based frame interpolation for video. In *Proceedings of the IEEE conference on computer vision and pattern recognition*, pages 1410–1418, 2015.
- [40] Vincent Michalski, Roland Memisevic, and Kishore Konda. Modeling deep temporal dependencies with recurrent grammar cells. In *Advances in neural information processing systems*, pages 1925–1933, 2014.
- [41] Roni Mittelman, Benjamin Kuipers, Silvio Savarese, and Honglak Lee. Structured recurrent temporal restricted boltzmann machines. In *International Conference on Machine Learning*, pages 1647–1655, 2014.
- [42] Santiago E Montesdeoca, Hock Soon Seah, Pierre Bénéard, Romain Vergne, Joëlle Thollot, Hans-Martin Rall, and Davide Benvenuti. Edge-and substrate-based effects for watercolor stylization. In *Proceedings of the Symposium on Non-Photorealistic Animation and Rendering*, page 2. ACM, 2017.
- [43] Simon Niklaus and Feng Liu. Context-aware synthesis for video frame interpolation. In *Proceedings of the IEEE Conference on Computer Vision and Pattern Recognition*, pages 1701–1710, 2018.
- [44] Simon Niklaus, Long Mai, and Feng Liu. Video frame interpolation via adaptive separable convolution. In *Proceedings of the IEEE International Conference on Computer Vision*, pages 261–270, 2017.
- [45] MarcAurelio Ranzato, Arthur Szlam, Joan Bruna, Michael Mathieu, Ronan Collobert, and Sumit Chopra. Video (language) modeling: a baseline for generative models of natural videos. *arXiv preprint arXiv:1412.6604*, 2014.
- [46] Olaf Ronneberger, Philipp Fischer, and Thomas Brox. U-net: Convolutional networks for biomedical image segmentation. In *International Conference on Medical image computing and computer-assisted intervention*, pages 234–241. Springer, 2015.
- [47] Tim Salimans, Ian Goodfellow, Wojciech Zaremba, Vicki Cheung, Alec Radford, and Xi Chen. Improved techniques for training gans. In *Advances in neural information processing systems*, pages 2234–2242, 2016.
- [48] Karen Simonyan and Andrew Zisserman. Very deep convolutional networks for large-scale image recognition. *arXiv preprint arXiv:1409.1556*, 2014.
- [49] Ilya Sutskever, Geoffrey E Hinton, and Graham W Taylor. The recurrent temporal restricted boltzmann machine. In *Advances in neural information processing systems*, pages 1601–1608, 2009.
- [50] Dizan Vasquez and Thierry Fraichard. Motion prediction for moving objects: a statistical approach. In *IEEE International Conference on Robotics and Automation, 2004. Proceedings. ICRA'04. 2004*, volume 4, pages 3931–3936. IEEE, 2004.
- [51] Ruben Villegas, Jimei Yang, Yuliang Zou, Sungryull Sohn, Xunyu Lin, and Honglak Lee. Learning to generate long-term future via hierarchical prediction. In *ICML*, 2017.
- [52] Carl Vondrick, Hamed Pirsiavash, and Antonio Torralba. Generating videos with scene dynamics. In *Advances In Neural Information Processing Systems*, pages 613–621, 2016.
- [53] Jacob Walker, Carl Doersch, Abhinav Gupta, and Martial Hebert. An uncertain future: Forecasting from static images using variational autoencoders. In *European Conference on Computer Vision*, pages 835–851. Springer, 2016.
- [54] Jacob Walker, Abhinav Gupta, and Martial Hebert. Patch to the future: Unsupervised visual prediction. In *Proceedings of the IEEE Conference on Computer Vision and Pattern Recognition*, pages 3302–3309, 2014.
- [55] Miaoyi Wang, Bin Wang, Yun Fei, Kanglai Qian, Wenping Wang, Jiating Chen, and Jun-Hai Yong. Towards photo watercolorization with artistic verisimilitude. *IEEE transactions on visualization and computer graphics*, 20(10):1451–1460, 2014.
- [56] Der-Lor Way and Zen-Chung Shih. The Synthesis of Rock Textures in Chinese Landscape Painting. *Computer Graphics Forum*, 2001.
- [57] Manuel Werlberger, Thomas Pock, Markus Unger, and Horst Bischof. Optical flow guided tv-l1 video interpolation and restoration. In *International Workshop on Energy Minimization Methods in Computer Vision and Pattern Recognition*, pages 273–286. Springer, 2011.

- [58] Ning Xie, Hirotaka Hachiya, and Masashi Sugiyama. Artist agent: A reinforcement learning approach to automatic stroke generation in oriental ink painting. *CoRR*, abs/1206.4634, 2012.
- [59] Ning Xie, Tingting Zhao, Feng Tian, Xiaohua Zhang, and Masashi Sugiyama. Stroke-based stylization learning and rendering with inverse reinforcement learning. In *Proceedings of the 24th International Conference on Artificial Intelligence, IJCAI'15*, pages 2531–2537. AAAI Press, 2015.
- [60] Jun Xing, Hsiang-Ting Chen, and Li-Yi Wei. Autocomplete painting repetitions. *ACM Transactions on Graphics (TOG)*, 33(6):172, 2014.
- [61] Songhua Xu, Min Tang, Francis Lau, and Yunhe Pan. A solid model based virtual hairy brush. In *Computer Graphics Forum*, volume 21, pages 299–308. Wiley Online Library, 2002.
- [62] Tianfan Xue, Jiajun Wu, Katherine Bouman, and Bill Freeman. Visual dynamics: Probabilistic future frame synthesis via cross convolutional networks. In *Advances in neural information processing systems*, pages 91–99, 2016.
- [63] Xinchun Yan, Jimei Yang, Kihyuk Sohn, and Honglak Lee. Attribute2image: Conditional image generation from visual attributes. In *European Conference on Computer Vision*, pages 776–791. Springer, 2016.
- [64] Zhefei Yu, Houqiang Li, Zhangyang Wang, Zeng Hu, and Chang Wen Chen. Multi-level video frame interpolation: Exploiting the interaction among different levels. *IEEE Transactions on Circuits and Systems for Video Technology*, 23(7):1235–1248, 2013.
- [65] Richard Zhang, Phillip Isola, Alexei A Efros, Eli Shechtman, and Oliver Wang. The unreasonable effectiveness of deep features as a perceptual metric. In *Proceedings of the IEEE Conference on Computer Vision and Pattern Recognition*, pages 586–595, 2018.
- [66] Yong Zhang, Weiming Dong, Chongyang Ma, Xing Mei, Ke Li, Feiyue Huang, Bao-Gang Hu, and Oliver Deussen. Data-driven synthesis of cartoon faces using different styles. *IEEE Transactions on image processing*, 26(1):464–478, 2017.
- [67] Ming Zheng, Antoine Milliez, Markus Gross, and Robert W Sumner. Example-based brushes for coherent stylized renderings. In *Proceedings of the Symposium on Non-Photorealistic Animation and Rendering*, page 3. ACM, 2017.
- [68] Yipin Zhou and Tamara L. Berg. Learning temporal transformations from time-lapse videos. volume 9912, pages 262–277, 10 2016.
- [69] Jun-Yan Zhu, Taesung Park, Phillip Isola, and Alexei A Efros. Unpaired image-to-image translation using cycle-consistent adversarial networks. In *Proceedings of the IEEE international conference on computer vision*, pages 2223–2232, 2017.

Appendix A. ELBO derivation

We provide the full derivation of our model and losses from Equation (3). We start with our goal of finding model parameters θ that maximize the following probability for all videos and all t :

$$\begin{aligned} & p_\theta(\delta_t, x_{t-1}; x_T) \\ & \propto p_\theta(\delta_t | x_{t-1}; x_T) \\ & = \int_{z_t} p_\theta(\delta_t | z_t, x_{t-1}; x_T) p(z_t) dz_t. \end{aligned}$$

We use variational inference and introduce an approximate posterior distribution $q_\phi(z_t | \delta_t, x_{t-1}; x_T)$ [32, 62, 63].

$$\begin{aligned} & \int_{z_t} p_\theta(\delta_t | z_t, x_{t-1}; x_T) p(z_t) dz_t \\ & = \int_{z_t} p_\theta(\delta_t | z_t, x_{t-1}; x_T) p(z_t) \frac{q_\phi(z_t | \delta_t, x_{t-1}; x_T)}{q_\phi(z_t | \delta_t, x_{t-1}; x_T)} dz_t \\ & \propto \log \int_{z_t} p_\theta(\delta_t | z_t, x_{t-1}; x_T) p(z_t) \frac{q_\phi(z_t | \delta_t, x_{t-1}; x_T)}{q_\phi(z_t | \delta_t, x_{t-1}; x_T)} dz_t \\ & = \log \int_{z_t} \frac{p_\theta(\delta_t | z_t, x_{t-1}; x_T) p(z_t)}{q_\phi(z_t | \delta_t, x_{t-1}; x_T)} q_\phi(z_t | \delta_t, x_{t-1}; x_T) dz_t \\ & = \log \mathbb{E}_{z_t \sim q_\phi(z_t | \delta_t, x_{t-1}; x_T)} \left[\frac{p_\theta(\delta_t | z_t, x_{t-1}; x_T) p(z_t)}{q_\phi(z_t | \delta_t, x_{t-1}; x_T)} \right]. \quad (8) \end{aligned}$$

We use the shorthand $z_t \sim q_\phi$ for $z \sim q_\phi(z_t | \delta_t, x_{t-1}; x_T)$, and apply Jensen's inequality:

$$\begin{aligned} & \log \mathbb{E}_{z_t \sim q_\phi} \left[\frac{p_\theta(\delta_t | z_t, x_{t-1}; x_T) p(z_t)}{q_\phi(z_t | \delta_t, x_{t-1}; x_T)} \right] \\ & \geq \mathbb{E}_{z_t \sim q_\phi} \left[\log p_\theta(\delta_t | z_t, x_{t-1}; x_T) \right] \\ & \quad + \mathbb{E}_{z_t \sim q_\phi} \left[\log \frac{p(z_t)}{q_\phi(z_t | \delta_t, x_{t-1}; x_T)} \right] \\ & \geq \mathbb{E}_{z_t \sim q_\phi} \left[\log p_\theta(\delta_t | z_t, x_{t-1}; x_T) \right] \\ & \quad - KL[q_\phi(z_t | \delta_t, x_{t-1}; x_T) || p(z_t)], \quad (9) \end{aligned}$$

where $KL[\cdot || \cdot]$ is the Kullback-Liebler divergence, arriving at the ELBO presented in Equation (5) in the paper.

Combining the first term in Equation (5) with our image likelihood defined in Equation (1):

$$\begin{aligned} & \mathbb{E}_{z_t \sim q_\phi} \log p_\theta(\delta_t | z_t, x_{t-1}; x_T) \\ & \propto \mathbb{E}_{z_t \sim q_\phi} \left[\log e^{-\frac{1}{\sigma_1^2} |\delta_t - \hat{\delta}_t|} \right. \\ & \quad \left. + \log \mathcal{N}(V(x_{t-1} + \delta_t); V(x_{t-1} + \hat{\delta}_t), \sigma_2^2 \mathbb{I}) \right] \\ & = \mathbb{E}_{z_t \sim q_\phi} \left[-\frac{1}{\sigma_1^2} |\delta_t - \hat{\delta}_t| \right. \\ & \quad \left. + \log \frac{1}{\sqrt{2\pi\sigma_2^2}} \exp\left(-\frac{(V(x_{t-1} + \delta_t) - V(x_{t-1} + \hat{\delta}_t))^2}{2\sigma_2^2}\right) \right] \\ & \propto \mathbb{E}_{z_t \sim q_\phi} \left[-\frac{1}{\sigma_1^2} |\delta_t - \hat{\delta}_t| \right. \\ & \quad \left. - \frac{1}{2\sigma_2^2} (V(x_{t-1} + \delta_t) - V(x_{t-1} + \hat{\delta}_t))^2 \right], \quad (10) \end{aligned}$$

giving us the image similarity losses in Equation (6). We derive \mathcal{L}_{KL} in Equation (6) by similarly taking the logarithm of the normal distributions defined in Equations (2) and (4).

Appendix B. Network architecture

We provide details about the architecture of our recurrent model and our critic model in Figure 13.

Appendix C. Human study

We surveyed 150 human participants. Each participant took a survey containing a training section followed by 14 questions.

Calibration: We first trained the participants by showing them several examples of real digital and watercolor painting time lapses.

Evaluation: We then showed each participant 14 pairs of time lapse videos, comprised of a mix of watercolor and digital paintings selected randomly from the test sets. Although each participant only saw a subset of the test paintings, every test painting was included in the surveys. Each pair contained videos of the same center-cropped painting. The videos were randomly chosen from all pairwise comparisons between real, *vdv*, and *ours*, with the ordering within each pair randomized as well. Samples from *vdv* and *ours* were generated randomly.

Validation: Within the survey, we also showed two repeated questions comparing a real video with a linearly interpolated video (which we described as *interp* in Table 2 in the paper) to validate that users understood the task. We did not use results from users who chose incorrect answers for one or both validation questions.

Appendix D. Additional results

We include additional qualitative results in Figures 14 and 15. We encourage the reader to view the supplementary video, which illustrates many of the discussed effects.

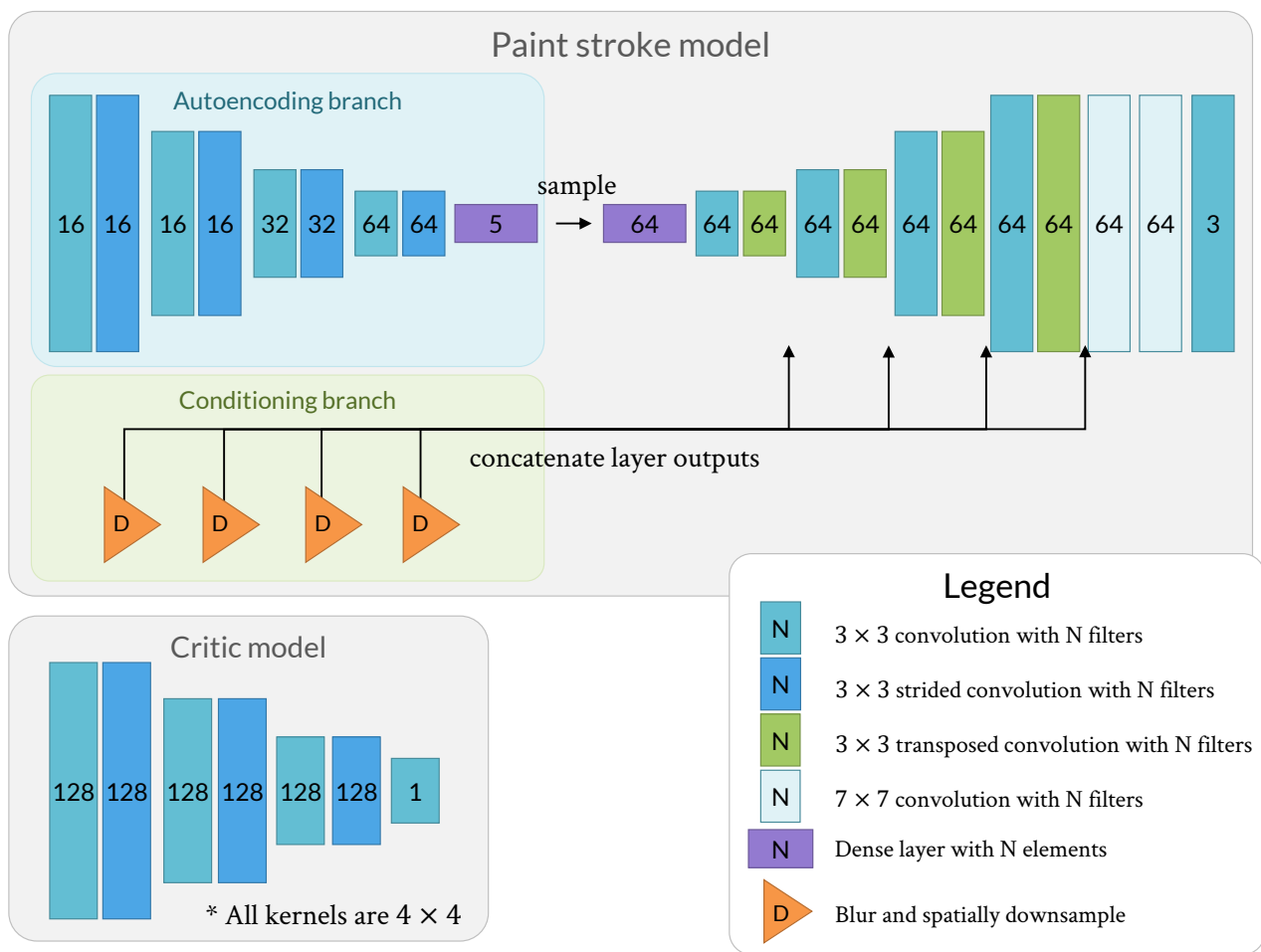
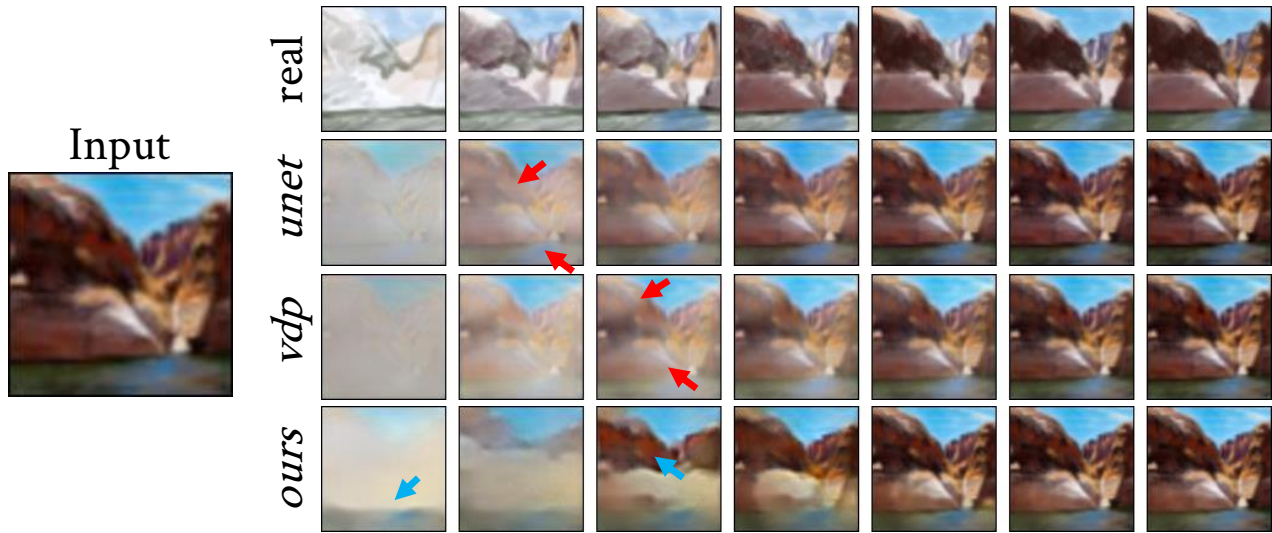


Figure 13: We use an encoder-decoder style architecture for our model. For our critic, we use a similar architecture to StarGAN [10], and optimize the critic using WGAN-GP [19] with a gradient penalty weight of 10 and 5 critic training iterations for each iteration of our model. All strided convolutions and downsampling layers reduce the size of the input volume by a factor of 2.

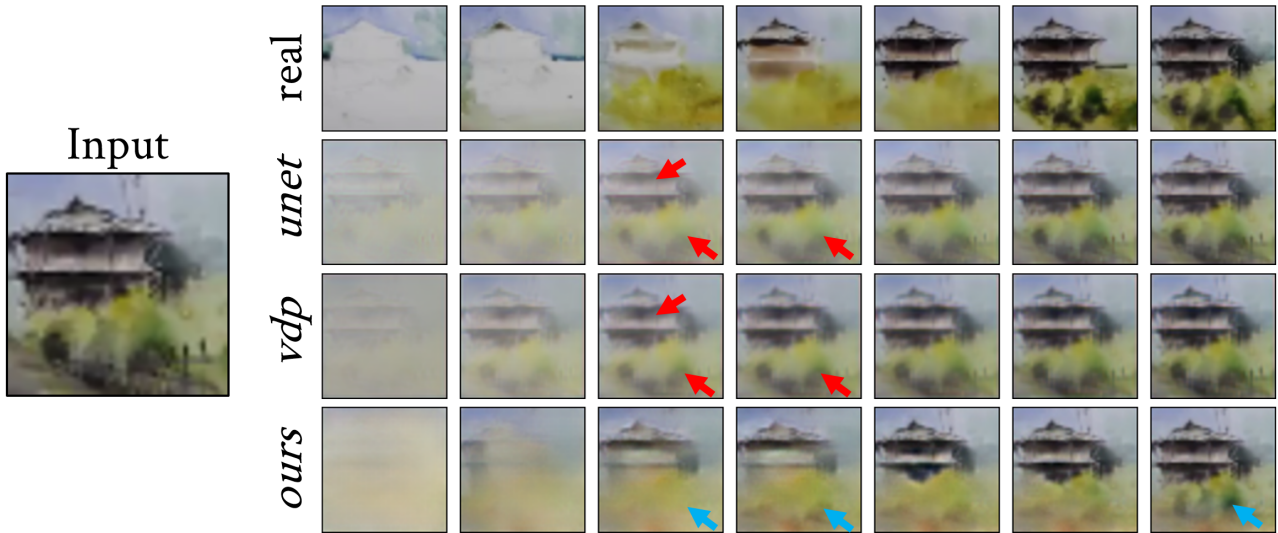


(a) **The proposed method paints similar regions to the artist.** Red arrows in the second row show where *unet* adds fine details everywhere in the scene, ignoring the semantic boundary between the rock and the water, and contributing to an unrealistic fading effect. The video synthesized by *vdp* uses more coarse strokes early on, but introduces an unrealistic-looking blurring and fading effect on the rock (red arrows in the third row). Blue arrows highlight that our method makes similar strokes to the artist, filling in the base color of the water, then the base colors of the rock, and then fine details throughout the painting.

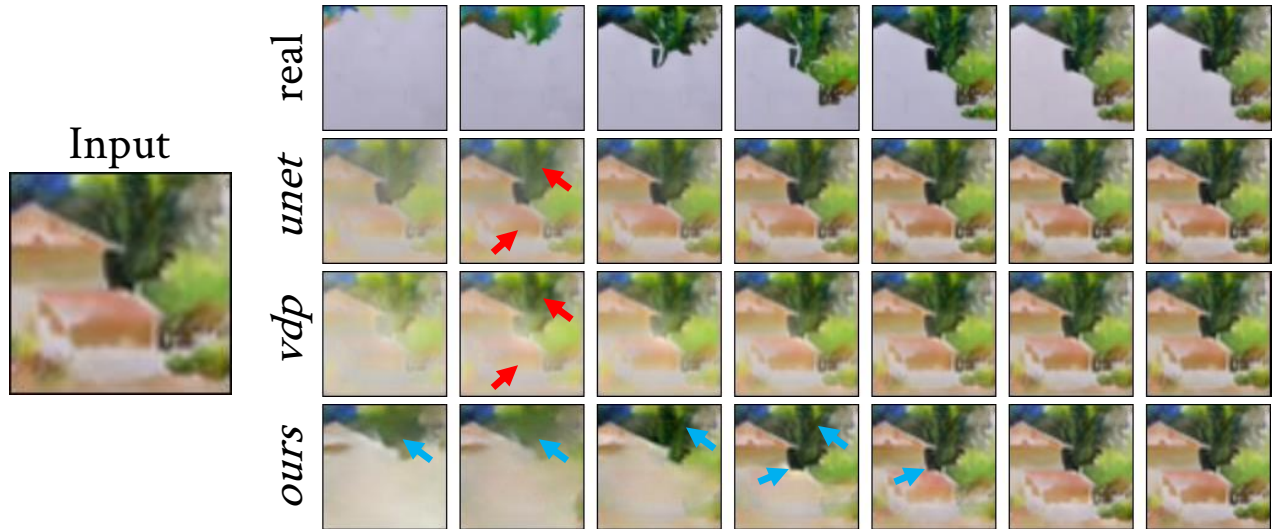


(b) **The proposed method identifies appropriate colors and shape for each layer of paint.** Red arrows indicate where the baselines fill in details that the artist does not complete until much later in the sequence (not shown in the real sequence, but visible in the input image). Blue arrows show where our method adds a base layer for the vase with a reasonable color and shape, and then adds fine details to it later.

Figure 14: Videos synthesized from the watercolor paintings test set. For the stochastic methods *vdp* and *ours*, we examine the nearest sample to the real video out of 2000 samples. We discuss the variability among samples from our method in Section 5, and in the supplementary video.



(a) **The proposed method paints using coarse-to-fine layers of different colors, similarly to the real artist.** Red arrows indicate where the baseline methods fill in details of the house and bush at the same time, adding fine-grained details even early in the painting. Blue arrows highlight where our method makes similar strokes to the artist, adding a flat base color for the bush first before filling in details, and using layers of different colors.



(b) **The proposed method synthesizes watercolor-like effects such as paint fading as it dries.** Red arrows indicate where the baselines fill in the house and the background at the same time. Blue arrows in the first two video frames of the last row show that our method uses coarse strokes early on. Blue arrows in frames 3-5 show where our method simulates paint drying effects (with the intensity of the color fading over time), which are common in real watercolor videos.

Figure 15: Videos synthesized from the watercolor paintings test set. For the stochastic methods *vdp* and *ours*, we show the nearest sample to the real video out of 2000 samples.